Heme Attachment Motif Mobility Tunes Cytochrome *c* Redox Potential†

Lea V. Michel,‡ Tao Ye,§ Sarah E. J. Bowman,|| Benjamin D. Levin,|| Megan A. Hahn,|| Brandy S. Russell,||,⊥ Sean J. Elliott,§ and Kara L. Bren*,||

Department of Biochemistry and Biophysics, University of Rochester, Rochester, New York 14642, Department of Chemistry, Boston University, Boston, Massachusetts 02215, and Department of Chemistry, University of Rochester, Rochester, New York 14627-0216

Received June 14, 2007; Revised Manuscript Received August 9, 2007

ABSTRACT: Hydrogen exchange (HX) rates and midpoint potentials (E_m) of variants of cytochrome *c* from *Pseudomonas aeruginosa* (*Pa* cyt c_{551}) and *Hydrogenobacter thermophilus* (*Ht* cyt c_{552}) have been characterized in an effort to develop an understanding of the impact of properties of the Cys-X-X-Cys-His pentapeptide *c*-heme attachment (CXXCH) motif on heme redox potential. Despite structural conservation of the CXXCH motif, *Ht* cyt c_{552} exhibits a low level of protection from HX for amide protons within this motif relative to *Pa* cyt c_{551}. Site-directed mutants have been prepared to determine the structural basis for and functional implications of these variations on HX behavior. The double mutant *Ht*-M13V/K22M displays suppressed HX within the CXXCH motif as well as a decreased E_m (by 81 mV), whereas the corresponding double mutant of *Pa* cyt c_{551} (V13M/M22K) exhibits enhanced HX within the CXXCH pentapeptide and a modest increase in E_m (by 30 mV). The changes in E_m correlate with changes in axial His chemical shifts in the ferric proteins reflecting the extent of histidinate character. Thus, the mobility of the CXXCH pentapeptide is found to impact the His−Fe(III) interaction and therefore the heme redox potential.

Electron transfer reactions involving iron-protoporphyrin IX (heme) are central to fundamental biological processes such as respiration, redox catalysis, sensing, and signaling (*1*−*5*). A key parameter determining the energetics and kinetics of electron transfer is the redox potential (*1*); thus, much emphasis has been placed on understanding the role of protein structure in tuning heme redox potential. Two fundamental features known to have a substantial influence on heme redox potentials are the nature of the ligands coordinated to the metal and the burial of the heme in the hydrophobic protein core. Nature alters the electron donating properties of the coordinating ligands through the choice of ligands (*6*) and by modulating metal−ligand bond strength (*6*−*12*), varying coordination geometry (*5*), and bonding of hydrogen to ligands (*13*−*15*). The encapsulation of the heme within a protein's interior also is significant for determining potential, as the hydrophobic environment favors the ferrous state over the ferric (*7*, *8*, *10*, *16*, *17*). Although there have been many studies of the effects of static polypeptide structure on heme−ligand interactions and on heme burial, the role of protein mobility has received less attention. Protein motions may indeed be important as they could influence metal−ligand interactions (*15*, *18*, *19*) and solvent exposure.

Here, we investigate the effects of structural fluctuations of the *c*-heme motif of cytochrome *c* (cyt *c*)[1] on redox potential. The *c*-type heme is characterized by its covalent attachment to the polypeptide, usually to two Cys residues in a Cys-X-X-Cys-His (CXXCH) pentapeptide motif, in which X may be any amino acid and His is a heme axial ligand [termed the proximal His (Figure 1A)] (*4*, *20*). The hypothesis tested in this study is that variations of sequence within and near the *c*-heme motif impact the energetics of the motif's conformational fluctuations, which in turn impact heme−ligand interactions and thus heme redox potential. The subjects of study are the soluble monoheme cyt *c* from *Hydrogenobacter thermophilus* (*Ht* cyt c_{552}) and that from *Pseudomonas aeruginosa* (*Pa* cyt c_{551}). Although these homologues display highly similar folds and structures at the CXXCH motif [residues 12−16 using *Pa* cyt c_{551} numbering (Figure 1)] (*21*, *22*), energetics of conformational fluctuations involving this pentapeptide, revealed by hydrogen exchange (HX), are surprisingly disparate. In particular, protection from HX of the amide protons of CXXCH motif residues Cys15 and His16, which donate hydrogen bonds to the Cys12 carbonyl (Figure 1B), differs greatly between these proteins. Mutations are introduced to test the roles of

† This work was supported by National Institutes of Health Grant GM63170 (K.L.B.), a fellowship from the Alfred P. Sloan Foundation (K.L.B.), and National Science Foundation Grant MCB-0546323 (S.J.E.).

* To whom correspondence should be addressed: Department of Chemistry, University of Rochester, Rochester, NY 14627-0216. Tel.: (585) 275-4335. Fax: (585) 276-0205. E-mail: bren@chem.rochester.edu.

‡ Department of Biochemistry and Biophysics, University of Rochester.

§ Department of Chemistry, Boston University.

|| Department of Chemistry, University of Rochester.

⊥ Current address: Department of Chemistry, Gustavus Adolphus College, St. Peter, MN 56082.

[1] Abbreviations: cyt *c*, cytochrome *c*; E_m, electrochemical midpoint potential; *Ht* cyt c_{552}, *Hydrogenobacter thermophilus* cytochrome c_{552}; HX, hydrogen exchange; NMR, nuclear magnetic resonance; *Pa* cyt c_{551}, *Pseudomonas aeruginosa* cytochrome c_{551}; PDB, Protein Data Bank; PFV, protein film voltammetry; rmsd, root-mean-square deviation.

10.1021/bi701177j CCC: $37.00
Published on Web 09/28/2007

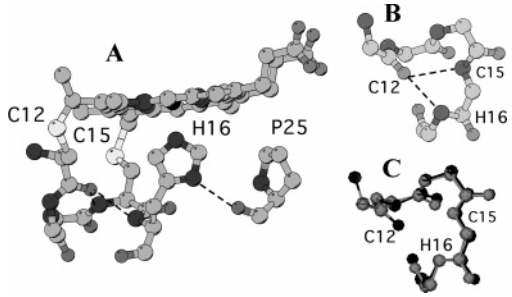

FIGURE 1: (A) Heme and CXXCH motif (residues 12−16) and Pro25 from *Pa* cyt c_{551} (PDB entry 351C) (*21*). The side chains of residues 13−15 have been omitted for clarity. The hydrogen bond between the Pro25 carbonyl group and the proximal His16 Hδ1 is represented by a dashed line. Panels A and B were prepared using Molscript (*65*). (B) Structure of the CXXCH motif from *Pa* cyt c_{551}. The intramotif hydrogen bonds between the Cys12 carbonyl and the backbone HN groups of Cys15 and His16 are represented by dashed lines. In panels A and B, nitrogen atoms are colored dark gray, oxygen atoms medium gray, and sulfur atoms the lightest shade of gray. (C) Overlay (rmsd of 0.21 Å) of the backbone of the CXXCH motif from *Pa* cyt c_{551} (silver) and *Ht* cyt c_{552} (black) (PDB entry 1YNR) (*22*). Panel C was prepared using VMD (*66*).

individual amino acids in modulating CXXCH motif fluctuations and the resulting effects on redox potential. The results indicate that the conformational dynamics of the CXXCH motif play a role in tuning heme potential by influencing the His−Fe interaction.

MATERIALS AND METHODS

Protein Expression and Purification. Plasmids pETPA (Amp^r) (*23*, *24*) and pSCH552 (Amp^r) (*25*) were used as templates for site-directed mutagenesis of *Pa* cyt c_{551} and *Ht* cyt c_{552}, respectively. Mutants (*Pa*-V13M, *Pa*-M22K, *Pa*-V13M/M22K, *Ht*-M13V, *Ht*-K22M, and *Ht*-M13V/K22M) were prepared using the QuikChange II kit (Stratagene). *Ht* cyt c_{552} and *Pa* cyt c_{551} were expressed and purified as previously described for the wild-type proteins (*23*, *25*). Preparation of uniformly ^{15}N-labeled proteins was by expression on minimal medium containing [^{15}N,99%]NH_4Cl (Cambridge Isotope Laboratories, Inc.) as the sole nitrogen source as described previously (*23*, *26*).

Collection and Analysis of NOESY Data. All NMR data were collected on a Varian INOVA 500 MHz spectrometer (operating at 499.839 MHz for ^1H) at 299 K. Collection of NOESY and TOCSY spectra of oxidized *Ht*-M13V/K22M and *Pa*-V13M/M22K {3 mM in 50 mM NaP_i (pH 6.0), 5-fold molar excess in $K_3[Fe(CN)_6]$} for analysis of heme pocket structure was as described for wild-type proteins (*23*, *25*). Assignments were made using standard methods, assisted by assignments available in the literature (*23*, *25*, *27*).

Collection and Analysis of HX Data. HX was initiated by adding 500 mL of D_2O to ~14 mg of *Pa* cyt c_{551}, *Pa*-V13M, *Pa*-M22K, *Pa*-V13M/M22K, *Ht* cyt c_{552}, *Ht*-M13V, *Ht*-K22M, or *Ht*-M13V/K22M which had been lyophilized from H_2O containing a 5-fold excess of $K_3[Fe(CN)_6]$ in 50 mM NaP_i (pH 6.0). The measured pH* (uncorrected) after initiation of exchange was 6.1 for all samples. Acquisition of two-dimensional TOCSY or HSQC (of ^{15}N-labeled proteins) data commenced ~7 min after initiation of exchange. TOCSY spectra were collected (32 scans, 4096 × 256 points, recycle time of 1.1 s) without solvent suppression 8, 14, 19, 25, 30, 35, 40, 95, and 315 h after initiation of exchange. For *Ht* cyt c_{552}, TOCSY spectra also were collected 800, 1450, and 2650 h after initiation of exchange. Between NMR experiments, samples were kept at 299 K in a water bath. HX experiments were performed on ^{15}N-labeled protein samples prepared as described above by collecting 3 h of consecutive HSQC spectra (2048 × 32 points, recycle time of 1.5 s) at 299 K after initiation of exchange, followed by spectra ~7, ~16, and ~20 h after initiation. NMR data were processed using Felix 97 (Accelrys). Resonance assignments were determined using standard methods, assisted by published assignments (*23*, *27*, *28*). Peak intensities in TOCSY spectra were normalized using peaks of nonexchangeable protons as references. Cross-peak intensities at various delay times [$I(t)$] were plotted against delay time (t) and fit using KaleidaGraph (Synergy Software) to a three-parameter single-exponential equation [$I(t) = A + B \exp(-k_{obs}t)$] to determine k_{obs}, the observed proton exchange rate. It was verified that exchange occurred in the EX2 limit (*29*) by observation of the expected ~10-fold decrease in exchange rates at pH 5.0. Protons in *Ht* cyt c_{552} that exchanged too slowly for determination of an exchange rate were assigned an upper limit rate of 1.0×10^{-8} s^{-1}, which is consistent with the observation of a <10% peak intensity change by the last time point. Protection factors (P) were calculated, according to the EX2 mechanism, as $\log P = \log(1/K_{op})$, where $K_{op} = k_{obs}/k_{int}$, k_{int} is the intrinsic exchange rate for the "open" form, and k_{obs} is the observed exchange rate (*30*, *31*). Values for k_{int} were determined using SPHERE (http://www.fccc.edu/research/labs/roder/sphere/) (*29*, *31*). A caveat to remember for protection factor analysis in this study is that the k_{int} values determined using SPHERE assume an unstructured polypeptide. In the case of residues at and close to the *c*-heme motif, however, the open form will not resemble an unstructured polypeptide. Thus, protection factors may not accurately reflect the true K_{op} value. Nevertheless, the purpose of the analysis here is to detect and interpret changes in protection factors between cyt *c* variants rather than perform a quantitative analysis of the K_{op} values themselves. This comparative analysis is valid because it is expected that perturbations of k_{int} for *c*-heme motif residues relative to an unstructured polypeptide would be similar for the different variants and species as a result of the local conservation of structure at the *c*-heme motif. Analyses of the *Ht* cyt c_{552} (*22*) and the *Pa* cyt c_{551} (*21*) crystal structures were performed using the graphics program MOLecule analysis and MOLecule display (MOLMOL) (*32*).

NMR Detection of Axial His Nuclei. Super-WEFT spectra (*33*) of oxidized *Ht* cyt c_{552}, *Ht*-M13V, *Ht*-K22M, and *Ht*-M13V/K22M were collected {1−3 mM protein, 50 mM NaP_i (pH 7.0), a 5-fold excess of $K_3[Fe(CN)_6]$, and D_2O}. Side chain protons on the Met and His axial ligands have T_1 values between 2 and 5 ms and are thus readily identified in the super-WEFT spectra. HSQC spectra of uniformly ^{15}N-labeled samples of all variants in this study {1.5−2 mM samples, 50 mM NaP_i (pH 7.0), 10% D_2O, and a 5-fold excess of $K_3[Fe(CN)_6]$} were collected using J_{NH} values of 90 and 135 Hz. The larger J_{NH} corresponds to a shorter INEPT delay, enhancing detection of rapidly relaxing nuclei. The His16 Hδ1−Nδ cross-peak was identified by its enhancement in these spectra as well as its characteristic chemical shifts, consistent with the previously reported Hδ1 shift (*34*).

Protein Electrochemistry. Protein film voltammetry (PFV) of cyt *c* species was performed as previously described (*15*), with the following modifications. pH dependency studies were carried out in either a mixture of citrate and KP_i buffer (pH ranging from 2.6 to 5) or 50 mM KP_i buffer (pH 6 to 8), at concentrations that ensure that phosphate ion binding has a minimal impact on the proteins (*15*, *35*, *36*). Experiments conducted at scan rates higher than 500 mV/s were performed in a solution of 10 mM KP_i buffer (pH 7), in addition to 85 mM $NaNO_3$, resulting in a final ionic strength (I_{total}) of ~100 mM. Buffers were titrated with NaOH or HCl to the desired pH. The temperature of the system was maintained at 0 °C by connecting the water-jacketed electrochemical cell to a refrigerating circulator. The thermostated, electrochemical cell was housed in a Faraday cage. A polycrystalline gold wire (geometrical area of 3 mm^2) embedded in epoxy comprised the working electrode. A resin-body saturated calomel electrode (SCE, Accumet), located in a Luggin side arm containing 100 mM Na_2SO_4 and maintained at room temperature, was used as a reference. All potentials quoted herein are against the standard hydrogen electrode. A platinum wire acted as the counter electrode to complete the three-electrode configuration. Voltammetry was conducted with an Autolab electrochemical analyzer (PGSTAT 12, Eco Chemie, Utrecht, The Netherlands), equipped with ECD and ADC modules, and controlled by GPES software (Eco Chemie). Compensating for the IR drop within the cell was further achieved by using the IR positive feedback module of the PG-STAT 12 instrument, as needed. Electroactive protein films were generated as previously described (*15*), and all experiments were repeated at least three times. The collected data were subjected to analysis by subtracting a polynomial baseline to remove the nonfaradaic current. The interfacial electron transfer rate constant (k^0) was determined by trumpet plot analysis (peak position of the cathodic and anodic electrochemical signals, as a function of scan rate), as described by Armstrong and coworkers (*37*, *38*).

RESULTS

Hydrogen Exchange of Wild-Type Proteins. HX experiments probe the energetics of conformational openings that lead to exchange of amide protons that are sequestered from solvent in the "closed" (folded) form. In what is termed the EX2 limit, the observed HX rates (k_{obs}) can be translated into protection factors [$\log P = \log(k_{int}/k_{obs})$], where k_{int} is the intrinsic exchange rate for the open form (*30*, *31*). Protection factors in turn are related to the free energy of the conformational opening leading to exchange ($\Delta G_{op} = RT \ln P$) (*29*). *Ht* cyt c_{552} and *Pa* cyt c_{551} exhibit similar overall trends in protection factors, as expected from their highly homologous secondary and tertiary structures (Figure S1 of the Supporting Information). The enhanced stability of *Ht* cyt c_{552} is reflected in its generally higher level of protection of core residues relative to *Pa* cyt c_{551} (*39*, *40*). Proteins from thermophilic organisms, such as *Ht* cyt c_{552}, typically experience higher-energy unfolding events (both global and subglobal) that lead to HX, and thus higher protection factors, as compared to those of their mesophilic counterparts (*41*). For CXXCH motif residues, however, this trend is not followed, as *Pa* cyt c_{551} exhibits greater protection of Cys15 (>10-fold) and His16 [>100-fold (Table 1)], two residues forming key hydrogen bonds within this motif to Cys12 (Figure 1; CMACH sequence in *Ht* cyt c_{552} and CVACH sequence in *Pa* cyt c_{551}). HX analysis thus reveals that conformational excursions leading to exchange of Cys15 and His16 amide protons occur with a lower energy in *Ht* cyt c_{552} than in *Pa* cyt c_{551}.

Table 1: Log of Protection Factors (log *P*) for Selected Residues in Wild-Type and Mutant Proteins

	Pa cyt c_{551}				*Ht* cyt c_{552}			
residue	wild type	V13M	M22K	V13M/M22K	wild type	M13V	K22M	M13V/K22M
15	4.5	<4.4[a]	5.1	3.4	<3.4[b]	<4.4[a]	<4.4[a]	4.5
16	5.9	4.7	5.5	4.0	3.6	4.7	6.0	6.7
17	4.6	4.2	4.5	4.2	4.8	4.5	4.9	4.4

[a] Exchanged before 8 h (not detected in the first TOCSY spectrum), upper limit given. [b] Exchanged before 13 min (not detected in the first HSQC spectrum), upper limit given.

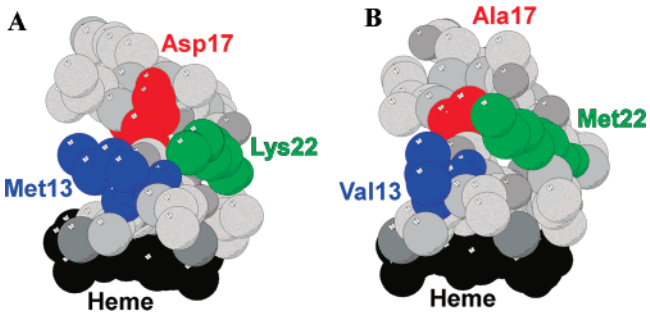

FIGURE 2: Space-filling representation of the proximal heme pocket of (A) *Ht* cyt c_{552} (PDB entry 1YNR) (*22*) and (B) *Pa* cyt c_{551} (PDB entry 351C) (*21*) highlighting residues targeted for mutation [residues 13 (blue) and 22 (green)] as well as residue 17 (red).

Hydrogen Exchange of Proximal Heme Pocket Mutants. The structures of the CXXCH pentapeptide backbone in *Pa* cyt c_{551} (*21*) and *Ht* cyt c_{552} (*22*) are nearly identical (see the next section). However, substantial differences in the level of protection of CXXCH backbone amide protons from HX are seen, suggesting that variations in proximal heme pocket residues influence energetics of CXXCH motif conformational openings leading to HX. Examination of the protein structures (*21*, *22*) (Figure 2) reveals that Met13 and Asp17 in *Ht* cyt c_{552} do not pack as well as Val13 and Ala17 do in *Pa* cyt c_{551}, which may destabilize the key interactions of Cys15 and His16 with Cys12 in *Ht* cyt c_{552} and result in more efficient exchange of the *Ht* cyt c_{552} His16 and Cys15 amide protons with solvent. Another notable difference is amino acid 22. In *Pa* cyt c_{551}, the hydrophobic Met22 lies across the CXXCH loop, which is expected to stabilize the loop against conformational openings. In *Ht* cyt c_{552}, residue 22 is Lys and as a charged residue may interact with solvent more than the loop region.

To test the hypothesized roles of residues 13 and 22 in influencing local conformational fluctuations, the mutants *Ht*-M13V, *Ht*-K22M, *Pa*-V13M, *Pa*-M22K, *Ht*-M13V/K22M, and *Pa*-V13M/M22K were prepared and HX rates were determined. If we focus on the double mutants which show the largest effects, overall backbone protection is similar between the mutants and their respective wild-type proteins (Figure S1). In the proximal pocket, however, significant decreases in the level of protection of Cys15 and His16 in *Pa*-V13M/M22K are seen relative to that of the wild type, and increases for these same residues are observed

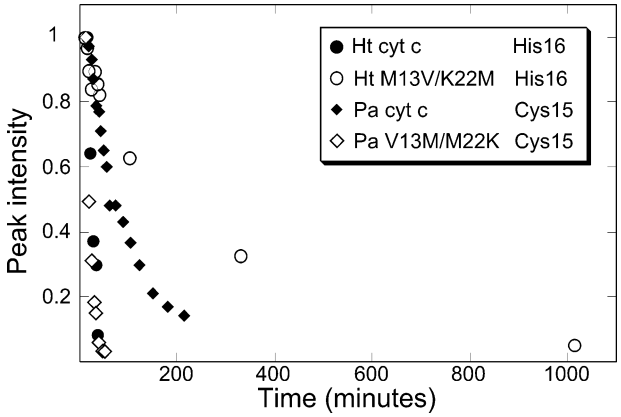

FIGURE 3: Representative peak intensity data from HX experiments. Shown are plots of peak intensity (normalized) vs time from HX initiation illustrating the difference in the observed HX rate between His16 in *Ht*-M13V/K22M (○) relative to *Ht* cyt c_{552} (●) and between Cys15 in *Pa*-V13M/M22K (◇) relative to *Pa* cyt c_{551} (◆).

for *Ht*-M13V/K22M relative to the wild type (Table 1). Particularly dramatic is the increase in the level of protection of His16 in *Ht*-M13V/K22M by more than 3 orders of magnitude relative to that of the wild type (Figure 3). These results indicate that residues 13 and 22, particularly in combination, play key roles in controlling the energetics of opening of the CXXCH motif in these proteins. Notably, the single mutants show intermediate changes in protection, in particular for *Ht* cyt c_{552} and its variants which show the more straightforward behavior relative to *Pa* cyt c_{552} (Table 1). Interestingly, protection of the Asp17 HN group, which hydrogen bonds to a buried water, shows little difference between the two cyt *c* species and among the mutants, suggesting that the differences seen here between proteins are specific to the CXXCH motif itself.

Analysis of c-Heme Motif Structures. To analyze the extent to which variations in the CXXCH sequence influence local backbone structure, 10 cyt *c* species having disparate properties of "XX" residues in the motif and for which high-resolution (<2.5 Å) X-ray crystal structures are available were selected for analysis (Table S1 of the Supporting Information). Despite differences in the variable XX residues, the CXXCH backbone structure is highly conserved, as it is defined primarily by the constraints of the covalent and coordinate bonds between the Cys and His residues with the heme (*42*, *43*). In the selected group of cyt *c* species, this motif displays a rmsd of 0.34 Å (for backbone atoms); *Ht* cyt c_{552} and *Pa* cyt c_{551} have a rmsd of 0.21 Å in this region (Figure 1C). Subtle structural differences are seen among the cyt *c* species, as illustrated by the modest range of distances between the backbone carbonyl oxygen of the first Cys in the motif (Cys12 in *Pa* cyt c_{551}) and its hydrogen bond donors Cys15 and His16 (Table S1). Nevertheless, despite wide sequence variations, the pentapeptide backbone structure is structurally conserved across diverse sequences.

To verify that the mutations introduced here do not significantly perturb CXXCH backbone structure, NOESY spectra for wild-type and double mutant proteins were compared, and the expected pattern of NOEs within the CXXCH motif between the wild-type and double mutant proteins is observed. (Results for *Ht*-M13V/K22M and the wild type are listed in Table S2 of the Supporting Information. A similar comparison of *Pa* cyt c_{551} and mutants was attempted, but extensive chemical shift degeneracy among residues 13−15 precluded a rigorous analysis.) The overall maintenance of the NOE pattern along with the strong conservation of the motif structure across diverse cyt *c* sequences and folds indicates that significant backbone structure rearrangement upon mutation is unlikely.

Assignment and Analysis of Proximal His NMR Resonances. Chemical shifts of heme axial His ring nuclei in paramagnetic heme proteins report on the His−Fe(III) interaction. The axial His16 Hδ1−Nδ1 HSQC peak for each protein is easily identified, as it is shifted outside of the diamagnetic envelope and exhibits an increase in intensity with increased J_{NH} values used in the HSQC experiment, which enhances detection of nuclei with short relaxation times as a result of their proximity to the paramagnetic iron. The Hϵ1 His proton resonance was identified for *Ht* cyt c_{552} and *Ht*-M13V/K22M using the one-dimensional super-WEFT experiment based on its very short T_1 and large upfield shift (*33*). Assignments for selected axial His nuclei are listed in Table 2, and a plot of His16 Hδ1 chemical shift versus E_m is shown in Figure 4. The Hϵ1 shift shows an increase in magnitude as E_m is lowered, reflecting increased histidinate character with a lower E_m (*44*−*49*). Likewise, the His16 Hδ1 shifts upfield as E_m is lowered, consistent with enhanced hydrogen bonding which has been demonstrated previously in other low-spin ferric heme proteins (*46*, *47*).

Protein Electrochemistry. The ability to modulate the energetics of conformational openings leading to HX of the CXXCH motif in *Ht* cyt c_{552} and *Pa* cyt c_{551} by selected mutations provides the opportunity to test the effects of fluctuations on heme redox potential to which HX is sensitive. Thus, the mutants were examined by protein film voltammetry (PFV) to determine the electrochemical midpoint potential (E_m) as well as the interfacial electron transfer kinetics. Table 3 summarizes the observed values of E_m at pH 7. Notably, the *Ht* cyt c_{552} mutants (single and double) display lower potentials: each of the mutations resulted in a systematic shift to lower potential that is nearly additive [$E_{WT} - E_{M13V/K22M}$ (81 mV) $\approx E_{WT} - E_{M13V}$ (59 mV) + ($E_{WT} - E_{K22M}$) (37 mV)]. To ensure this is not merely an effect of variable pH-dependent phenomena between the mutants, the impact of pH upon E_m for the *Ht* cyt c_{552} species was assessed (Figure 5). Clearly, all of the *Ht* cyt c_{552} species (wild-type and mutants) display potentials that are pH-independent close to pH 7. Further, the same simple model of protonation holds for each of the mutants considered here, where a single pK_{red} is observed for the reduced form of the various cyt *c* species, spanning a modest range of values from 4.2 to 4.7, and indicating that the mutations do not significantly alter the protonation associated with heme redox chemistry.

The *Pa* cyt c_{551} species also were investigated by PFV, and the midpoint potentials at pH 7 are given in Table 3. Compared to the case for the *Ht* cyt c_{552} mutants, a reversed trend is observed; however, the increases are smaller, and not additive as seen for the *Ht* cyt c_{552} mutants. This discrepancy may be due to differences in pH-dependent behavior, as it has been previously shown that the redox behavior of *Pa* cyt c_{551} mutants displays disrupted H^+:e^- coupling and pH dependencies of E_m that cannot be fit to previously described models of binding of protons to heme propionate 7 (*15*, *50*). Thus, a quantitative evaluation of the

Table 2: Chemical Shifts (parts per million) of Selected Axial His Nuclei at pH 7.0

	Pa cyt c_{551}				*Ht* cyt c_{552}			
nucleus	wild type	V13M	M22K	V13M/M22K	wild type	M13V	K22M	M13V/K22M
Nδ1	169.3	171.1	171.6	173.2	182.3	170.5	181.3	167.1
Hδ1	11.9	12.1	12.7	12.7	13.2	11.8	12.7	11.2
Hϵ1	—[a]	—[a]	—[a]	—[a]	−16.4[b]	−17.6	−16.1	−17.5

[a] Not assigned. [b] Consistent with the literature assignment (*34*).

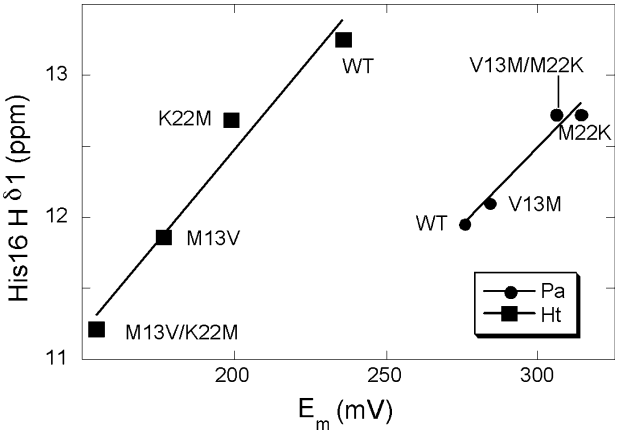

FIGURE 4: Plot of His16 Hδ1 chemical shift vs E_m for the wild-type (WT) proteins and six mutants. Data for *Pa* cyt c_{551} and mutants are plotted with circles, and data for *Ht* cyt c_{552} and mutants are plotted with squares. The lines demonstrate the linear fit and have the same slope as each other (0.02 ppm/mV) within error.

Table 3: Electrochemical Data for the Wild-Type and Mutant Proteins, Comparing the Midpoint Potentials at pH 7 and the Interfacial Electron Transfer Rates (k^0)

protein	variant	E_m at pH 7 (mV)	k^0 (s^{-1})
Pa cyt c_{551}	wild type	276 ± 2	1028 ± 117
	V13M	284 ± 2	1056 ± 142
	M22K	314 ± 2	921 ± 77
	V13M/M22K	306 ± 3	969 ± 119
Ht cyt c_{552}	wild type	236 ± 2	1007 ± 128
	M13V	177 ± 1	1025 ± 112
	K22M	199 ± 1	1240 ± 74
	M13V/K22M	155 ± 2	1027 ± 124

exact change in potential is challenging, although the qualitative trends are clear.

In parallel experiments, interfacial electron transfer rates for each of the cyt *c* species were determined by trumpet plot analysis (Figure S2 of the Supporting Information). All of the proteins display fast electron transfer, with k^0 being on the order of 10^3 s^{-1} (Table 3), which is similar to reported k^0 values for eukaryotic cyt *c* species investigated on gold electrodes (*51*−*53*).

DISCUSSION

Electrochemical Response of Mutants. We have examined the relationship between cyt *c* mutations that impact the conformational openings of the CXXCH motif, and the redox properties of the resulting mutants. Relative to the wild type, the mutants of *Ht* cyt c_{552} that have suppressed HX show a systematic decrease in E_m, whereas those *Pa* cyt c_{551} species with enhanced HX display an increase in E_m. Before linking these changes in E_m to specific features of heme pocket mobility, we can consider several traits of the *Pa* cyt c_{551} and *Ht* cyt c_{552} mutants: electrostatic charge perturbations, alterations in the protein fold, proximal histidinate character, and heme conformation. For example, a possible explanation is that the observed changes in E_m could arise from electrostatic perturbations caused by the mutations. Specifically, the electrostatic potential at the heme iron can be influenced by the charges in surrounding residues (*54*, *55*). Here, for example, in *Ht*-M13V/K22M, the charged Lys side chain is replaced with a neutral side chain, Met. However, the charge-neutral single mutation, M13V, has a greater impact on redox potential than the K22M mutation (Table 3), thus suggesting that the change in the charge of residue 22 is not the major contributor to the significant decrease in redox potential exhibited by *Ht*-M13V/K22M. It also is notable that the cyt *c* species studied demonstrate reversible direct electrochemistry upon modified gold electrodes, indicative of rapid electron transfer kinetics (10^3 s^{-1}). Furthermore, the *Ht* cyt c_{552} mutants all behave like the wild type in terms of the previously characterized relationships between E_m and both phosphate ion and proton binding schemes (*15*). These general observations suggest that the observed changes in E_m result from fundamental differences in the heme pocket and not alterations in apparent electrokinetics, pH-induced effects, or electrostatics.

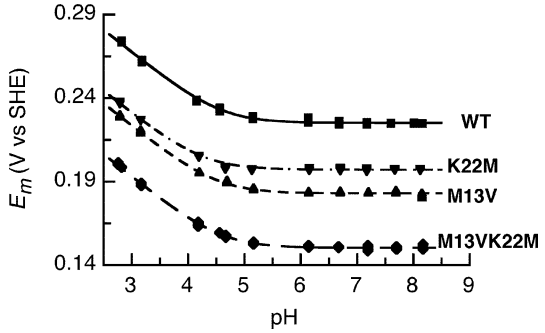

FIGURE 5: E_m values of four *Ht* cyt c_{552} species [wild type (■), M13V (▲), K22M (▼), and M13V/K22M (◆)] as determined by PFV at 0 °C, 50 mV/s, in phosphate-containing buffer, as a function of pH. All data were acquired using a scan rate of 50 mV/s. pK_{red} values for wild-type *Ht* cyt c_{552}, *Ht*-M13V, *Ht*-K22M, and *Ht*-M13V/K22M were found to be 4.2, 4.7, 4.2, and 4.3, respectively. Fitting was carried out as described previously (*15*).

Structure of Mutants. The changes in E_m for the mutants could be a result of alterations to the protein fold. The pattern of protection factors (with the exception of the proximal heme pocket residues) for the mutants is similar overall to that for the wild-type proteins; this finding argues against a global structure perturbation caused by mutation because protection from HX reflects hydrogen bonding and secondary structure (*56*) (Figure S2). Within the proximal heme pockets, the similarity of NOE patterns for the wild-type and mutant proteins argues against major local backbone structure changes (Table S2). Indeed, no major change in the structure

of the CXXCH motif upon mutation is expected as this structure is highly conserved among cyt *c* species despite wide variations in the identity of the XX and other heme pocket residues (Figure 1C and Table S1). In addition, the close similarity between the CXXCH structure in *c*-heme peptide fragments (microperoxidases) and that in folded cyt *c* indicates that local coordinate and covalent bonding defines the motif's three-dimensional backbone structure (*42*, *43*). Barring changes in local polypeptide folding causing the observed changes in E_m, we propose a model in which perturbations of the redox potential can be caused by alterations in CXXCH motif mobility impacting donor properties of the proximal His. Analysis of proximal His chemical shifts supports this hypothesis, as shown below. A second possible explanation discussed below is that mutations impact E_m by exerting a systematic change in heme conformation.

Effect of Mutations on Proximal His. The proximal His16 in *Ht* cyt c_{552} and *Pa* cyt c_{551} donates a hydrogen bond to the backbone carbonyl of Pro25, with an oxygen−nitrogen distance of ~2.8 Å (Figure 1A) (*21*, *22*). Hydrogen bonding involving the axial His in heme proteins has been shown to affect the ligand's electron donating properties, which in turn tunes redox potential (*13*, *14*, *44*, *46*, *47*, *57*). Specifically, the stronger the hydrogen bond between the His ligand Hδ1 and the hydrogen bond acceptor, the greater the histidinate character. A more appreciable histidinate character results in the His being a better donor of electrons to the iron, which stabilizes the ferric oxidation state more than the ferrous and hence provides for a decrease in redox potential. This effect has been analyzed previously by comparing the cyanide-inhibited forms of different heme proteins with different E_m values (*44*, *46*) or by mutating residues that hydrogen bond with a proximal His residue (*45*). Here, we examine a more indirect effect of local CXXCH motif structure on the proximal His in cyts *c* species.

Evaluation of the histidinate character of the proximal His and hydrogen bonding with the proximal His has been performed by analysis of its chemical shifts in the ferric state. The heme axial His Hδ1, the hydrogen bond donor, has been shown to display an upfield shift in the low-spin ferric proteins as E_m is lowered, with other factors remaining constant (*46*, *47*). A similar correlation is seen here for the lower-potential variants of *Ht* cyt c_{552} which exhibit a systematic upfield shift of the His16 Hδ1 (as well as Nδ) resonance compared to that of the wild type (Figure 4 and Tables 2 and 3). In a complementary fashion, the *Pa* cyt c_{551} mutants exhibit a downfield shift of His16 Hδ1 (and Nδ) relative to that of the wild type. Notably, the magnitude of the change in shift correlates well with the magnitude of the change in E_m, as illustrated by the similar slopes of the lines in Figure 4 (0.022 ± 0.003 and 0.025 ± 0.003 ppm/mV for *Pa* cyt c_{551} variants and *Ht* cyt c_{552} variants, respectively). The need to consider the shifts of each protein species separately is a result of differences in the pseudocontact contribution to chemical shift, as the two proteins have different heme axial Met orientations and thus different magnetic anisotropies and orientations of magnetic axes (*28*). Because of the large error in calculating the significant pseudocontact contribution to chemical shift for the His ligand, correction for this difference has not been made. The magnitude of the axial His Hϵ1 chemical shifts also has been related to the extent of histidinate character (*44*−*49*). In step with other results presented here, the *Ht* cyt c_{552} mutants generally display an upfield shift of His16 Hϵ1 relative to that of the wild type (Table 2). The His16 Hϵ1 of *Pa* cyt c_{551} could not be assigned.

We next consider how variations in CXXCH motif mobility reflected by HX may cause the observed differences in hydrogen bonding to the proximal His and the His−Fe(III) interaction. Changes in HX protection of the Cys15 and His16 amide protons directly report on conformational openings of the CXXCH motif as they form key hydrogen bonds with Cys12 carbonyl (Figure 1B). Thus, the greater protection of these residues in *Ht*-M13V/K22M relative to the wild type (Table 1) reflects a more rigid CXXCH structure with suppressed conformational excursions to an open form. Decreased CXXCH mobility in turn is correlated here with a lower E_m. A basis for the observed correlation is that higher CXXCH mobility interferes mechanically with the maintenance of the His16 Hδ1−Pro25 CO hydrogen bond, reducing histidinate character and increasing E_m for variants with enhanced HX. An alternative related explanation for the lower E_m in variants with suppressed HX is that more limited (transient) access of water to the proximal heme pocket enhances hydrogen bonding between His16 and Pro25 by excluding competing hydrogen bonding groups (water) and/or by decreasing the local dielectric.

A comparison of HX behavior of mitochondrial ferric cyt b_5 (OM b_5) to microsomal ferric cyt b_5 (Mc b_5) has previously invoked a role of heme pocket mobility in tuning redox potential (*18*). HX results reveal that OM b_5 undergoes higher-energy unfolding events in the heme pocket compared to Mc b_5, indicating less conformational mobility surrounding one of the His axial ligands in the former protein. The resulting tighter hydrophobic packing around the heme active site is proposed to yield stronger His−Fe(III) coordination in OM b_5, which may account for its lower redox potential (*18*). A similar effect has been invoked in a study of model heme−peptide compounds, in which high peptide mobility has been correlated with high redox potential. The high heme potential is proposed to result from preferential weakening of the His−Fe(III) bond relative to the His−Fe(II) bond (*19*).

Possible Role of Heme Conformation. Studies of *c*-heme peptides (microperoxidases) have shown that the CXXCH motif is sufficient to induce the significant distortion of heme from planarity toward the ruffled conformation that is typically seen in *c*-type cytochromes (*58*, *59*). In addition, an enhanced hydrophobic environment for this motif (provided by encapsulation of microperoxidase in a reverse micelle in model studies) is proposed to augment the buckling force of the CXXCH pentapeptide on the heme by strengthening the characteristic backbone hydrogen bonds within the CXXCH motif (*58*, *60*). The changes in protection for the variants here may reflect a similar effect; the variants with suppressed HX have enhanced hydrogen bonding within the CXXCH motif, which may increase the degree of heme distortion. The increased degree of distortion, in turn, would decrease redox potential (*59*, *61*), consistent with our observations.

Summary. The extent of protection of the residues within the CXXCH region is highly variable among cyt *c* species, despite the conservation of local backbone structure. In particular, great variability is observed in the protection of

the backbone amide protons of the His axial ligand and the preceding Cys residue, defining the key intramotif hydrogen bonding interactions with the first Cys carbonyl (Figure 1B). (For examples of differences in protection among oxidized cyt *c* species, see refs *23* and *62*−*64*. Note that such comparisons must be made with caution as data were collected under a range of conditions.) The different propensities for conformational opening of the CXXCH motif, modulated by the identity of the variable residues within and near the signature pentapeptide, indeed may play a role in tuning heme redox potential by influencing His donor properties and/or heme conformation. Further studies of this possible relationship will be probed in the future by addressing the relative enthalpic and entropic contributions to E_m for the individual mutants. We conclude that variations in heme pocket mobility should be considered when accounting for factors impacting E_m (*18*, *19*) in addition to the "static" factors traditionally invoked.

ACKNOWLEDGMENT

We are grateful to Linda Thöny-Meyer for the gift of pEC86 and Francesca Cutruzzolà for the gift of pETPA.

SUPPORTING INFORMATION AVAILABLE

One table listing information about 10 cyt *c* species utilized in analysis of CXXCH structure, one table listing CXXCH NOEs for *Ht* cyt c_{552} and *Ht*-M13V/K22M, one figure showing protection factors for wild-type and double-mutant proteins, and one figure showing a trumpet plot for *Ht*-M13V/K22M. This material is available free of charge via the Internet at http://pubs.acs.org.

REFERENCES

1. Marcus, R. A., and Sutin, N. (1985) Electron transfers in chemistry and biology, *Biochim. Biophys. Acta 811*, 265−322.
2. Gray, H. B., and Winkler, J. R. (2003) Electron tunneling through proteins, *Q. Rev. Biophys. 36*, 341−372.
3. Paoli, M., Marles-Wright, J., and Smith, A. (2002) Structure-function relationships in heme-proteins, *DNA Cell Biol. 21*, 271−280.
4. Bertini, I., Cavallaro, G., and Rosato, A. (2006) Cytochrome *c*: Occurrence and functions, *Chem. Rev. 106*, 90−115.
5. Walker, F. A. (2004) Models of the bis-histidine-ligated electron-transferring cytochromes. Comparative geometric and electronic structure of low-spin ferro- and ferrihemes, *Chem. Rev. 104*, 589−615.
6. Raphael, A. L., and Gray, H. B. (1991) Semisynthesis of axial ligand (position-80) mutants of cytochrome *c*, *J. Am. Chem. Soc. 113*, 1038−1040.
7. Tezcan, F. A., Winkler, J. R., and Gray, H. B. (1998) Effects of ligation and folding on reduction potentials of heme proteins, *J. Am. Chem. Soc. 120*, 13383−13388.
8. Mao, J. J., Hauser, K., and Gunner, M. R. (2003) How cytochromes with different folds control heme redox potentials, *Biochemistry 42*, 9829−9840.
9. Kennedy, M. L., Silchenko, S., Houndonougbo, N., Gibney, B. R., Dutton, P. L., Rodgers, K. R., and Benson, D. R. (2001) Model hemoprotein reduction potentials: The effects of histidine-to-iron coordination equilibrium, *J. Am. Chem. Soc. 123*, 4635−4636.
10. Battistuzzi, G., Bellei, M., Borsari, M., Di Rocco, G., Ranieri, A., and Sola, M. (2005) Axial ligation and polypeptide matrix effects on the reduction potential of heme proteins probed on their cyanide adducts, *J. Biol. Inorg. Chem. 10*, 643−651.
11. Cowley, A. B., Lukat-Rodgers, G. S., Rodgers, K. R., and Benson, D. R. (2004) A possible role for the covalent heme-protein linkage in cytochrome *c* revealed via comparison of N-acetylmicroperoxidase-8 and a synthetic, monohistidine-coordinated heme peptide, *Biochemistry 43*, 1656−1666.
12. Reedy, C. J., and Gibney, B. R. (2004) Heme protein assemblies, *Chem. Rev. 104*, 617−649.
13. O'Brien, P., and Sweigart, D. A. (1985) Effect on redox potentials of hydrogen bonding from coordinated imidazole in metalloporphyrin complexes, *Inorg. Chem. 24*, 1405−1409.
14. Quinn, R., Mercer-Smith, J., Burstyn, J. N., and Valentine, J. S. (1984) Influence of hydrogen bonding on the properties of iron porphyrin imidazole complexes: An internally hydrogen-bonded imidazole ligand, *J. Am. Chem. Soc. 106*, 4136−4144.
15. Ye, T., Kaur, R., Wen, X., Bren, K. L., and Elliott, S. J. (2005) Redox properties of wild-type and heme-binding loop mutants of bacterial cytochromes *c* measured by direct electrochemistry, *Inorg. Chem. 44*, 8999−9006.
16. Churg, A. K., and Warshel, A. (1986) Control of the redox potential of cytochrome *c* and microscopic dielectric effects in proteins, *Biochemistry 25*, 1675−1681.
17. Shifman, J. M., Gibney, B. R., Sharp, R. E., and Dutton, P. L. (2000) Heme redox potential control in de novo designed four-α-helix bundle proteins, *Biochemistry 39*, 14813−14821.
18. Simeonov, M., Altuve, A., Massiah, M. A., Wang, A., Eastman, M. A., Benson, D. R., and Rivera, M. (2005) Mitochondrial and microsomal ferric *b*-5 cytochromes exhibit divergent conformational plasticity in the context of a common fold, *Biochemistry 44*, 9308−9319.
19. Cowley, A. B., Kennedy, M. L., Silchenko, S., Lukat-Rodgers, G. S., Rodgers, K. R., and Benson, D. R. (2006) Insight into heme protein redox potential control and functional aspects of six-coordinate ligand-sensing heme proteins from studies of synthetic heme peptides, *Inorg. Chem. 45*, 9985−10001.
20. Scott, R. A., and Mauk, A. G. (1996) *Cytochrome c: A Multidisciplinary Approach*, University Science Books, Sausalito, CA.
21. Matsuura, Y., Takano, T., and Dickerson, R. E. (1982) Structure of cytochrome *c*-551 from *Pseudomonas aeruginosa* refined at 1.6-Å resolution and comparison of the 2 redox forms, *J. Mol. Biol. 156*, 389−409.
22. Travaglini-Allocatelli, C., Gianni, S., Dubey, V. K., Borgia, A., Di Matteo, A., Bonivento, D., Cutruzzolà, F., Bren, K. L., and Brunori, M. (2005) An obligatory intermediate in the folding pathway of cytochrome *c*-552 from *Hydrogenobacter thermophilus*, *J. Biol. Chem. 280*, 25729−25734.
23. Russell, B. S., Zhong, L., Bigotti, M. G., Cutruzzolà, F., and Bren, K. L. (2003) Backbone dynamics and hydrogen exchange of *Pseudomonas aeruginosa* ferricytochrome *c*-551, *J. Biol. Inorg. Chem. 8*, 156−166.
24. Wen, X., and Bren, K. L. (2005) Heme axial methionine fluxion in *Pseudomonas aeruginosa* Asn64Gln cytochrome *c*-551, *Inorg. Chem. 44*, 8587−8593.
25. Karan, E. F., Russell, B. S., and Bren, K. L. (2002) Characterization of *Hydrogenobacter thermophilus* cytochromes *c*-552 expressed in the cytoplasm and periplasm of *Escherichia coli*, *J. Biol. Inorg. Chem. 7*, 260−272.
26. Morar, A. S., Kakouras, D., Young, G. B., Boyd, J., and Pielak, G. J. (1999) Expression of N-15-labeled eukaryotic cytochrome *c* in *Escherichia coli*, *J. Biol. Inorg. Chem. 4*, 220−222.
27. Timkovich, R., and Cai, M. L. (1993) Investigation of the structure of oxidized *Pseudomonas aeruginosa* cytochrome *c*-551 by NMR: Comparison of observed paramagnetic shifts and calculated pseudocontact shifts, *Biochemistry 32*, 11516−11523.
28. Zhong, L., Wen, X., Rabinowitz, T. M., Russell, B. S., Karan, E. F., and Bren, K. L. (2004) Heme axial methionine fluxionality in *Hydrogenobacter thermophilus* cytochrome *c*-552, *Proc. Natl. Acad. Sci. U.S.A. 101*, 8637−8642.
29. Englander, S. W., and Kallenbach, N. R. (1983) Hydrogen exchange and structural dynamics of proteins and nucleic acids, *Q. Rev. Biophys. 16*, 521−655.
30. Hvidt, A., and Nielsen, S. O. (1966) Hydrogen exchange in proteins, *Adv. Protein Chem. 21*, 287−386.
31. Bai, Y. W., Milne, J. S., Mayne, L., and Englander, S. W. (1993) Primary structure effects on peptide group hydrogen exchange, *Proteins 17*, 75−86.
32. Koradi, R., Billeter, M., and Wüthrich, K. (1996) MOLMOL: A program for display and analysis of macromolecular structures, *J. Mol. Graphics 14*, 51.
33. Inubushi, T., and Becker, E. D. (1983) Efficient detection of paramagnetically shifted NMR resonances by optimizing the WEFT pulse sequence, *J. Magn. Reson. 51*, 128−133.
34. Tachiiri, N., Hemmi, H., Takayama, S. J., Mita, H., Hasegawa, J., Sambongi, Y., and Yamamoto, Y. (2004) Effects of axial

methionine coordination on the in-plane asymmetry of the heme electronic structure of cytochrome *c*, *J. Biol. Inorg. Chem. 9*, 733−742.
35. Brautigan, D. L., Ferguson-Miller, S. G., and Margoliash, E. (1978) Definition of cytochrome *c* binding domains by chemical modification. I. Reaction with 4-chloro-3,5-dinitrobenzoate and chromatographic separation of singly substituted derivatives, *J. Biol. Chem. 253*, 130−139.
36. Margalit, R., and Schejter, A. (1973) Cytochrome *c*: Thermodynamic study of relationships among oxidation state, ion-binding, and structural parameters. 1. Effects of temperature, pH and electrostatic media on standard redox potential of cytochrome *c*, *Eur. J. Biochem. 32*, 492−499.
37. Armstrong, F. A., Camba, R., Heering, H. A., Hirst, J., Jeuken, L. J. C., Jones, A. K., Léger, C., and McEvoy, J. P. (2000) Fast voltammetric studies of the kinetics and energetics of coupled electron-transfer reactions in proteins, *Faraday Discuss.*, 191−203.
38. Hirst, J., and Armstrong, F. A. (1998) Fast-scan cyclic voltammetry of protein films on pyrolytic graphite edge electrodes: Characteristics of electron exchange, *Anal. Chem. 70*, 5062−5071.
39. Uchiyama, S., Ohshima, A., Nakamura, S., Hasegawa, J., Terui, N., Takayama, S. I. J., Yamamoto, Y., Sambongi, Y., and Kobayashi, Y. (2004) Complete thermal unfolding profiles of oxidized and reduced cytochromes *c*, *J. Am. Chem. Soc. 126*, 14684−14685.
40. Wen, X., Patel, K. M., Russell, B. S., and Bren, K. L. (2007) Effects of heme pocket structure and mobility on cytochrome *c* stability, *Biochemistry 46*, 2537−2544.
41. Závodszky, P., Kardos, J., Svingor, Á., and Petsko, G. A. (1998) Adjustment of conformational flexibility is a key event in the thermal adaptation of proteins, *Proc. Natl. Acad. Sci. U.S.A. 95*, 855−871.
42. Low, D. W., Gray, H. B., and Duus, J. Ø. (1997) Paramagnetic NMR spectroscopy of microperoxidase-8, *J. Am. Chem. Soc. 119*, 1−5.
43. Ma, J. G., Laberge, M., Song, X. Z., Jentzen, W., Jia, S. L., Zhang, J., Vanderkooi, J. M., and Shelnutt, J. A. (1998) Protein-induced changes in nonplanarity of the porphyrin in nickel cytochrome *c* probed by resonance Raman spectroscopy, *Biochemistry 37*, 5118−5128.
44. La Mar, G. N., de Ropp, J. S., Chacko, V. P., Satterlee, J. D., and Erman, J. E. (1982) Axial histidyl imidazole non-exchangeable proton resonances as indicators of imidazole hydrogen-bonding in ferric cyanide complexes of heme peroxidases, *Biochim. Biophys. Acta 708*, 317−325.
45. Satterlee, J. D., Erman, J. E., Mauro, J. M., and Kraut, J. (1990) Comparative proton NMR analysis of wild-type cytochrome *c* peroxidase from yeast, the recombinant enzyme from *Escherichia coli*, and an Asp235Asn mutant, *Biochemistry 29*, 8797−8804.
46. Banci, L., Bertini, I., Turano, P., Tien, M., and Kirk, T. K. (1991) Proton NMR investigation into the basis for the relatively high redox potential of lignin peroxidase, *Proc. Natl. Acad. Sci. U.S.A. 88*, 6956−6960.
47. Banci, L., Bertini, I., Kuan, I. C., Tien, M., Turano, P., and Vila, A. J. (1993) NMR investigation of isotopically labeled cyanide derivatives of lignin peroxidase and manganese peroxidase, *Biochemistry 32*, 13483−13489.
48. Ferrer, J. C., Turano, P., Banci, L., Bertini, I., Morris, I. K., Smith, K. M., Smith, M., and Mauk, A. G. (1994) Active-site coordination chemistry of the cytochrome *c* peroxidase Asp235Ala variant: Spectroscopic and functional characterization, *Biochemistry 33*, 7819−7829.
49. de Ropp, J. S., Sham, S., Asokan, A., Newmyer, S., de Montellano, P. R. O., and La Mar, G. N. (2002) Influence of the distal His in imparting imidazolate character to the proximal His in heme peroxidase: H-1 NMR spectroscopic study of cyanide-inhibited His42 → Ala horseradish peroxidase, *J. Am. Chem. Soc. 124*, 11029−11037.
50. Leitch, F. A., Moore, G. R., and Pettigrew, G. W. (1984) Structural basis for the variation of pH-dependent redox potentials of *Pseudomonas* cytochromes *c*-551, *Biochemistry 23*, 1831−1838.
51. Song, S., Clark, R. A., Bowden, E. F., and Tarlov, M. J. (1993) Characterization of cytochrome *c* alkanethiolate structures prepared by self-assembly on gold, *J. Phys. Chem. 97*, 6564−6572.
52. Avila, A., Gregory, B. W., Niki, K., and Cotton, T. M. (2000) An electrochemical approach to investigate gated electron transfer using a physiological model system: Cytochrome *c* immobilized on carboxylic acid-terminated alkanethiol self-assembled monolayers on gold electrodes, *J. Phys. Chem. B 104*, 2759−2766.
53. Niki, K., Hardy, W. R., Hill, M. G., Li, H., Sprinkle, J. R., Margoliash, E., Fujita, K., Tanimura, R., Nakamura, N., Ohno, H., Richards, J. H., and Gray, H. B. (2003) Coupling to lysine-13 promotes electron tunneling through carboxylate-terminated alkanethiol self-assembled monolayers to cytochrome *c*, *J. Phys. Chem. B 107*, 9947−9949.
54. Gunner, M. R., and Honig, B. (1991) Electrostatic control of midpoint potentials in the cytochrome subunit of the *Rhodopseudomonas viridis* reaction center, *Proc. Natl. Acad. Sci. U.S.A. 88*, 9151−9155.
55. Voigt, P., and Knapp, E. W. (2003) Tuning heme redox potentials in the cytochrome *c* subunit of photosynthetic reaction centers, *J. Biol. Chem. 278*, 51993−52001.
56. Milne, J. S., Mayne, L., Roder, H., Wand, A. J., and Englander, S. W. (1998) Determinants of protein hydrogen exchange studied in equine cytochrome *c*, *Protein Sci. 7*, 739−745.
57. Goodin, D. B., and McRee, D. E. (1993) The Asp-His-Fe triad of cytochrome *c* peroxidase controls the reduction potential, electronic structure, and coupling of the tryptophan free radical to the heme, *Biochemistry 32*, 3313−3324.
58. Ma, J. G., Vanderkooi, J. M., Zhang, J., Jia, S. L., and Shelnutt, J. A. (1999) Resonance Raman investigation of nickel microperoxidase-11, *Biochemistry 38*, 2787−2795.
59. Jentzen, W., Ma, J. G., and Shelnutt, J. A. (1998) Conservation of the conformation of the porphyrin macrocycle in hemoproteins, *Biophys. J. 74*, 753−763.
60. Ma, J. G., Zhang, J., Franco, R., Jia, S. L., Moura, I., Moura, J. J. G., Kroneck, P. M. H., and Shelnutt, J. A. (1998) The structural origin of nonplanar heme distortions in tetraheme ferricytochromes *c*-3, *Biochemistry 37*, 12431−12442.
61. Barkigia, K. M., Chantranupong, L., Smith, K. M., and Fajer, J. (1988) Structural and theoretical models of photosynthetic chromophores: Implications for redox, light-absorption properties and vectorial electron flow, *J. Am. Chem. Soc. 110*, 7566−7567.
62. Bartalesi, I., Rosato, A., and Zhang, W. (2003) Hydrogen exchange in a bacterial cytochrome *c*: A fingerprint of the cytochrome *c* fold, *Biochemistry 42*, 10923−10930.
63. Marmorino, J. L., Auld, D. S., Betz, S. F., Doyle, D. F., Young, G. B., and Pielak, G. J. (1993) Amide proton exchange rates of oxidized and reduced *Saccharomyces cerevisiae* iso-1-cytochrome *c*, *Protein Sci. 2*, 1966−1974.
64. Bai, Y. W., Sosnick, T. R., Mayne, L., and Englander, S. W. (1995) Protein folding intermediates: Native state hydrogen exchange, *Science 269*, 192−197.
65. Kraulis, P. J. (1991) Molscript: A program to produce both detailed and schematic plots of protein structures, *J. Appl. Crystallogr. 24*, 946−950.
66. Humphrey, W., Dalke, A., and Schulten, K. (1996) VMD: Visual molecular dynamics, *J. Mol. Graphics 14*, 33.

BI701177J